Upscaling solute transport in naturally fractured porous media with the Continuous Time Random Walk Method

S. Geiger,[1] A. Cortis,[2] and J. T. Birkholzer[2]

S. Geiger, Institute of Petroleum Engineering, Heriot-Watt University, Edinburgh, EH14 4AS, U.K.

(sebastian.geiger@pet.hw.ac.uk)

A. Cortis, J. T. Birkholzer, Earth Sciences Division, Lawrence Berkeley National Laboratory, University of California, Berkeley, CA 94720, USA.

[1]Institute of Petroleum Engineering, Heriot-Watt University, Edinburgh, U.K.

[2]Earth Sciences Division, Lawrence Berkeley National Laboratory, Berkeley, California, USA.

Abstract. Solute transport in fractured porous media is typically "non-Fickian", i.e. it is characterized by early breakthrough and long tailing, and by nonlinear growth of the Green function centered second moment. This behavior is due to the effects of (1) multi-rate diffusion occurring between the highly permeable fracture network and the low permeability rock matrix and (2) a wide range of advection rates in the fractures and, possibly, the matrix as well, (3) a range of path lengths. As a consequence prediction of solute transport processes at the macro scale represents a formidable challenge. Classical dual porosity (or mobile-immobile) approaches in conjunction with an advection dispersion equation and macroscopic dispersivity commonly fail to predict breakthrough of fractured porous media accurately. It was recently demonstrated that the Continuous Time Random Walk (CTRW) method can be used as a generalized upscaling approach. Here we extend this work and use results from high-resolution finite element – finite volume based simulations of solute transport in an outcrop analogue of a naturally fractured reservoir to calibrate the CTRW method by extracting a distribution of retention times. This procedure allows us to predict breakthrough at other model locations accurately and gain significant insight into the nature of the fracture-matrix interaction in naturally fractured porous reservoirs with geologically realistic fracture geometries.

1. Introduction

Fractured porous formations are often found in geological reservoirs. Yet, the accurate prediction of solute transport in fractured porous formations is very challenging because an exact description of the geometry and connectivity of the network of connected fractures in the subsurface remains elusive [Bonnet et al., 2001; Berkowitz, 2002]. Open and well-connected fractures comprise high-permeability pathways and are orders of magnitude more permeable than the porous rock matrix. Typically transport velocities in fractures and matrix vary over several orders of magnitude [Matthäi and Belayneh, 2004]. Traditionally, fractured porous media are hence separated into two distinct flow domains: The high-permeability (mobile) domain, the network of connected fractures where solute transport occurs predominantly by advection, and the low-permeability (almost-immobile) domain, the rock matrix where solute transport is generally dominated by diffusion. The rock matrix also provides the storage capacity for solutes because its pore volume is significantly larger than the fracture volume. The presence of two flow domains causes steep concentration gradients between fractures and matrix because solute concentrations change more rapidly in the fractures compared to the rock matrix. This local disequilibrium in solute concentration gives rise to dominantly diffusive exchange between fracture and matrix which, together with variable flow rates in the fractures and matrix themselves, causes "non-Fickian" breakthrough curves characterized by early breakthrough and long tailing, and by nonlinear growth of the Green function centered second moment. Hence it must be accounted for and predicted accurately at the macro-scale (upscaled), that is at the scale of a groundwater aquifer or hydrocarbon reservoir. In this work, the

term “upscaling” is intended as a procedure aimed at extrapolating (over time and space) the evolution of the concentration over similar scales, under an assumption of stationarity for the structure of the heterogeneity field. As such, the use of “upscaling” in this work should not misconstrued with averaging procedures aimed at calculating effective transport properties such as porosity and/or permeability over several decades in scale.

The classical upscaling approach to model fluid flow in fractured porous media at the reservoir scale is to invoke the so-called “dual-porosity” approach [Barenblatt et al., 1960; Warren and Root, 1963]. It assumes that fluid flow occurs only in the mobile fracture domain, for which an effective permeability must be computed. The matrix domain is immobile. Both domains are connected via a simple linear transfer function. The transfer function accounts for the exchange of fluid across the boundary of the two domains. The transfer function contains a shape factor that accounts for the geometry of this boundary. Extensions of the classical dual-porosity concept have been developed to model solute transport in fractured porous media. Solute transport in the mobile domain is represented by an effective transport velocity and macro-dispersivity, whereas solute diffusion between the immobile and mobile regions is approximated with first-order transfer terms [Huyakorn et al., 1983a; Birkholzer and Rouve, 1994; McDermott et al., 2009], higher-order transfer terms [Bibby, 1981; Huyakorn et al., 1983b, c; Dykhuizen, 1990; Zimmerman et al., 1990, 1993; Birkholzer and Rouve, 1994], multi-continuum models [Lichtner and Kang, 2007], linear Boltzmann transport equation [Benke and Painter, 2003; Painter and Cvetkovic, 2005], or by using a distribution of transfer rates [Haggerty and Gorelick, 1995; Feehley et al., 2000; Flach et al., 2004; Berkowitz et al., 2008].

However, there are some fundamental assumptions underlying dual-porosity models which are known to restrict their applicability to represent real fracture networks at the continuum scale. First, it is assumed that the fractures possess a well-defined representative elementary volume such that effective transport properties – most notably an effective permeability – can be computed for the mobile domain. However, this is usually only true for idealized geometries of fracture networks. Natural fractures patterns commonly possess a representative elementary volume only at the scale of the entire reservoir because they are often poorly-connected, their length distribution follows a power-law behavior, and fracture aperture is positively correlated to fracture length [Bonnet et al., 2001; Berkowitz, 2002]. Hence flow rates in the fracture network itself are highly variable and can give rise to "non-Fickian" transport, even with limited or no solute exchange between fracture and matrix [Berkowitz and Scher, 1995, 1997, 1998; Berkowitz et al., 2001; Kosakowski et al., 2001]. Such breakthrough curves cannot be modeled with a single effective transport velocity and macro-dispersivity. Secondly, recent studies have demonstrated that the diffusive exchange between fracture and matrix is inherently of multi-rate nature and hence must be modeled by an adequate multi-rate mass transfer formulation because adequate calibration of a dual-porosity model cannot be achieved otherwise and simulated breakthrough curves will differ significantly from the ones measured in the field [Haggerty et al., 2000; McKenna et al., 2001]. It was also shown that the advective transport component in more permeable matrix blocks (e.g., porous sandstones) results in additional solute transfer between fractures and matrix, which is not typically taken into account by dual porosity concepts [Cortis and Birkholzer, 2008].

The Continuous Time Random Walk (CTRW) method is an alternative to the classical dual-porosity models for modeling and upscaling flow and/or solute transport in fractured rock masses [Berkowitz and Scher, 1995, 1997, 1998; Noetinger and Estebenet, 2000; Berkowitz et al., 2001; Kosakowski et al., 2001; Noetinger et al., 2001a, b; Berkowitz et al., 2008; Cortis and Birkholzer, 2008]. Originally developed to describe electron hopping in heterogeneous physical systems [Scher and Lax, 1973a, b], the CTRW method has now become an efficient and accurate method to model solute transport in heterogeneous porous media Berkowitz et al. [2006], and a more insightful alternative to Monte Carlo approaches [Painter and Cvetkovic, 2005]. The multi-scale distribution of low- and high-permeability regions inherent to natural (fractured) porous media leads to local retardation and acceleration of solute transport, respectively, and "non-Fickian" (or anomalous) transport, which cannot be modeled with classical concepts of transport in homogeneous porous media [Cortis et al., 2004a]. The CTRW method has been applied to explain and model solute and heat transport in heterogeneous porous media. Applications range from the pore- [Bijeljic et al., 2004; Bijeljic and Blunt, 2006] and core-scale [Cortis and Berkowitz, 2004] to the reservoir-scale [Di Donato et al., 2003; Rhodes et al., 2008, 2009] and include the flow and transport of emulsions [Cortis and Ghezzehei, 2007], bio-colloids [Cortis et al., 2006], and heat transfer [Emmanuel and Berkowitz, 2007; Geiger and Emmanuel, 2010]. Mathematically, (dual-porosity) models with multi-rate mass transfer between mobile and immobile regions are equivalent to the CTRW method [Dentz and Berkowitz, 2003; Berkowitz et al., 2008], but the latter can also account for advection in the matrix [Cortis and Birkholzer, 2008].

A third approach are discrete-fracture-and-matrix (DFM) models. They can be used to simulate single- and multiphase transport in fractured porous media while explicitly accounting for the geometry of geometrically complex and non-orthogonally intersecting fractures. Hence the contribution of each individual fracture to fluid flow, including flow at fracture intersections and fracture terminations, is captured in the numerical model. This is usually achieved by a finite element or finite volume methods, or a combination of both. The dimensionality of the fractures is reduced from d to $d-1$, that is the fractures are lines in two-dimensional models or two-dimensional surfaces in three-dimensional models. Each lower-dimensional finite element/finite volume representing a fracture comprises its own permeability and transmissibility that corresponds to the prescribed fracture aperture [Kim and Deo, 2000; Juanes et al., 2002; Karimi-Fard and Firoozabadi, 2003; Geiger et al., 2004; Karimi-Fard et al., 2004; Monteagudo and Firoozabadi, 2004; Hoteit and Firoozabadi, 2005; Niessner et al., 2005; Reichenberger et al., 2006; Matthäi et al., 2007; Paluszny et al., 2007; Hoteit and Firoozabadi, 2008a, b; Haegland et al., 2009]. Since the contribution of each individual fractures to fluid flow and solute transport is accounted for directly, effective permeabilities, macro-dispersivities, and transfer functions for the entire fracture network do not need to be computed. However, the method is computationally not as efficient as a dual-porosity model or the CTRW method because fractures with very high flow rates must be discretized individually, which is a significant challenge in 3D and can lead to high computational costs. Although the DFM is powerful in analyzing the emergent behavior of transport in fractured porous media, their calibration to breakthrough curves measured in the field is still difficult. Since the exact description of the fracture geometry and connectivity is impossible from limited subsurface data [Bonnet

et al., 2001; Berkowitz, 2002], fracture networks must to be generated statistically until the breakthrough curves simulated with the DFM approach match the ones observed in the field. However, the statistical generation of a three-dimensional fracture network also requires the remeshing of the discrete fractures and matrix, which is a time-consuming process [Assteerawatt, 2008].

In this paper we evaluate the applicability of the CTRW method for upscaling solute transport in geologically realistic fractured porous media, including the accurate representation of the solute exchange between the mobile fracture and immobile matrix region. The work extends the earlier studies by Cortis and Birkholzer [2008] where the CTRW method was used to analyse solute transport and tracer breakthrough for idealized fracture-matrix geometries. Here we employ a state-of-the-art DFM simulation technique [Geiger et al., 2004; Paluszny et al., 2007; Matthäi et al., 2010] to simulate the transport of an inert chemical solute in a highly-detailed representation of fracture geometries mapped in the Bristol Channel, U. K. [Belayneh, 2004], a unique analogue for naturally fractured reservoirs. These simulations are used as surrogates to generate "correct" breakthrough curves from which we extract a residence time distribution with a non-parametric inversion best fit solution of the CTRW method [Cortis, 2007]. This residence time distribution is equivalent to the upscaling information and allows us to forecast the breakthrough curves at other locations in the model accurately.

The paper is organized as follows: In the next section we describe the geological model and the simulation at the continuum scale. This is followed by a description of the resulting breakthrough curves and concentration distributions. We then discuss the analysis of the breakthrough curves using the CTRW method and how this approach can be used in an

upscaling approach. We close by discussing our results in the wider context of upscaling solute transport in fractured porous media.

2. Continuum-Scale Modeling

2.1. Outcrop Analogue and Model Setup

The model geometry for our simulations utilizes the Triassic limestones fracture patterns exposed at the southern margin of the Bristol Channel coast in the U.K. (Figure 1a). While a limited number outcrops of the Bristol Channel exhibit mineralized fractures, that is the fractures have lower permeability than the rock matrix and are probably baffles to flow, we specifically focus on those outcrops were fractures are open and have significantly higher (usually by orders of magnitude) permeabilities than the rock matrix and are hence flow conduits. Because the fractures in this outcrop are bound to individual beds, usually only several tens of centimeters high, a two-dimensional plane-view geometry is used, that is gravity is neglected in the simulations. Model dimensions are 18×8 m^2. The fracture patterns from the Bristol Channel have been used previously for numerical analysis of single- and multi-phase flow in fractured reservoir analogues [Matthäi and Belayneh, 2004; Belayneh et al., 2006; Geiger et al., 2009; Matthäi et al., 2010; Geiger and Emmanuel, 2010].

The model specifications and properties are given in Table 1. Unlike the fracture geometry, these are not based on field data but chosen to explore a wide parameter range for a geologically realistic fracture-matrix pattern. Fixed pressures of 10.01 and 10 bar, respectively, are applied to the inflow (left) and outflow (right) model boundaries, whereas a no-flow boundary condition is imposed on the lateral boundaries. This results in a heterogeneous pressure gradient decreasing from the left to the right model boundary and

hence solute transport is from left to right (Figure 1b). The concentration is held fixed at 1 kg cm^{-3} along the inflow model boundary. The concentration gradient at the outflow boundary and the two horizontal boundaries is set to $\partial c/\partial x = 0$, respectively $\partial c/\partial y = 0$. Two cases are considered for the fracture aperture: (1) The fracture aperture varies between 0.1 and 1.2 mm, giving rise to spatially varying fracture permeabilities, k_f. (2) The fracture aperture is uniform at 1 mm, giving rise to a uniform fracture permeability and less heterogeneity in fracture flow. The matrix permeability k_m is uniform in space and time but different values are used in different simulations. Matrix permeabilities are 10^{-11}, 10^{-13}, 10^{-15}, and 10^{-17} m^2 (Table 1), which encompasses permeable sedimentary rocks to impermeable crystalline rocks. The porosity is 1 in the fractures and 0.25 in the matrix. The longitudinal and transversal dispersivities are $\alpha_L = 0.01$ m and $\alpha_T = 0.001$ m, respectively. They are constant and uniform in the model and model dispersion occurring at the scale below the resolution of a single finite element. We tested if different dispersivity coefficients in the fracture and matrix influence the breakthrough curves but found that this only is a secondary effect. The pore diffusivity D is constant and uniform in the model at 10^{-9} m s^{-2}. Dispersivities and pore diffusivity combine to form the dispersion tensor $\mathbf{D}$ (Equation 4).

The breakthrough curves were measured as the flux-weighted concentrations along four vertical profiles at the non-dimensional distances $\chi = 0.25$ and, 0.5, 0.75, and 0.999. Here the horizontal distance from the left inflow boundary x was normalized by the total length of the domain L, i.e. $\chi = x/L$. We also define the following parameters: The non-dimensional time $\tau = L/(\hat{v}\hat{\phi})$ where $\hat{v}$ is the volume averaged horizontal flow rate through the model measured by the finite volume method and $\hat{\phi}$ is the averaged model porosity

given by the harmonic mean of the porosity in each finite element and the area of the finite element; $\hat{k}$ is the averaged horizontal model permeability given by $\hat{k} = (\hat{v}\mu)(L/\Delta P)$ where μ is the fluid viscosity and ΔP the horizontal pressure drop across the model (see Table 1); R is the ratio of volumetric flow in the fractures to volumetric flow in the matrix.

2.2. Governing Equations and Numerical Methods

We solve a steady state pressure equation for incompressible fluids in two dimensional plane view, that is neglecting gravity,

$$0 = \nabla \cdot \left[\frac{k(\mathbf{x})}{\mu} \nabla p \right], \tag{1}$$

where k is the locally varying permeability of the matrix or fracture, p is the fluid pressure, μ the fluid viscosity, and $\mathbf{x}$ is a vector of spatial coordinates. The local fracture permeability, k_f, is calculated from the local fracture aperture, a, using the parallel plate law and the corresponding assumption that the fractures are bounded smooth planar walls

$$k_f(\mathbf{x}) = \frac{(a(\mathbf{x}))^2}{12}. \tag{2}$$

For simplicity, the permeabilities are assumed to be scalar. The two-dimensional velocity field is obtained by solving Darcy's law

$$\vec{v}(\mathbf{x}) = -\frac{k(\mathbf{x})}{\mu} \nabla p. \tag{3}$$

Transport of an inert chemical component is modeled locally using the standard advection-dispersion-equation

$$\phi(\mathbf{x}) \frac{\partial c}{\partial t} = -\nabla \cdot [\vec{v}(\mathbf{x}) c - \mathbf{D}(\mathbf{x}) \nabla c] \tag{4}$$

where c is the concentration of the chemical component and ϕ and $\mathbf{D}$ are the local porosity and local dispersion tensor, respectively. We stress that the dispersion tensor $\mathbf{D}$ is only used to model dispersion below the scale of a single finite element.

The equations are solved numerically in a DFM approach using a combination of finite element and upwind-weighted finite volume methods [Geiger et al., 2004; Paluszny et al., 2007; Matthäi et al., 2010], which as implemented in the "Complex System Modeling Platform – CSMP++" [Matthäi et al., 2007]. The finite element method is used to solve the fluid pressure equation (Equation 1) and the diffusive part of the advection-dispersion equation (Equation 4). The finite volume method is used to solve the advective part of Equation 4. This allows us to use the numerical formulation that is best suited to solve a certain type of equations; the finite volume method for advection (hyperbolic) equations and the finite element method for diffusion (elliptic and parabolic) equations.

The geometry of the Bristol Channel outcrop (Figure 1a) is discretized using a mixed-dimensional finite element technique. The finite elements are isoparametric with linear basis functions. The finite volume cells are created around each corner node of the finite elements. One-dimensional line elements are used to represent the fractures and two-dimensional triangular finite elements are used to represent the matrix. The fracture permeabilities are scaled by the fracture aperture to obtain the correct transmissibility for the one-dimensional finite elements belonging to the fractures. A key advantage of our combination of finite element and finite volume methods is that the upwind-weighting of the finite volume method overcomes numerical stability issues related to the grid Péclet number for advection dominated flow. Hence we can use significantly coarser grids than the ones dictated by the grid Péclet number. In total 347k finite elements and 154k

nodes are used to discretize the domain. The minimum and maximum element areas are 7.3×10^{-7} m^2 and 2.0×10^{-2} m^2, respectively. Implicit time-stepping was used with a fixed time-step of 0.005 days. This is still a very fine spatial and temporal discretization which allows us to minimize numerical dispersion and resolve the concentration gradients between fracture and matrix accurately. We carried out several initial trial runs with varying grid refinements and time-steps to assess the impact of numerical dispersion on solute transport but found it to be small compared to physical dispersion as long as the time-step size is reasonably small [Matthäi et al., 2010]. We emphasize that the non-Gaussianity of the solute motion in the fracture network results thus from the fine spatial discretization and the interaction with the matrix elements. The algebraic multigrid solver SAMG was used to invert the resulting matrices of linear ordinary equations efficiently and accurately during each time-step [Stüben, 2001; Stüben and Clees, 2005].

3. Results

The mean transport characteristics, expressed in the averaged permeability $\hat{k}$, averaged velocity $\hat{v}$, and ratio of volumetric flow in the fracture and matrix R are listed in Table 2 for the cases with varying and uniform fracture apertures. Since the fractures are well-connected they already carry 30 times more flow compared to the matrix at a matrix permeability of 10^{-11} m^2 and have flow rates that are at least four orders of magnitude higher than in the matrix (Figure 2). Hence the $\hat{v}$ and $\hat{k}$ do not change significantly as the matrix permeability decreases from 10^{-11} to 10^{-17} m^2 ($\hat{k} \approx 3 \times 10^{-10}$ m^2 and $\hat{v} \approx 2 \times 10^{-5}$ m s-1). In other words, advective transport is dominated by the fractures even if the matrix is comparatively permeable and small variations in fracture aperture have only a minor effect on $\hat{v}$ and $\hat{k}$. Local variations in fracture aperture also do not impact these

averaged transport properties greatly; the case with uniform fracture apertures has slightly higher averaged transport characteristics due to the absence of small-aperture fractures.

Velocity histograms (Figure 2) for the fractures and matrix show that flow rates vary between four and ten orders of magnitude, which is also reflected in the R values (Table 2). Velocity histograms for the fractures are, generally, wider than the velocity histograms for the matrix (2.5 vs. 1.5 orders of magnitude variation in velocity, respectively). Note that the velocity histograms for the fracture are largely unaffected by variations in matrix permeability because the fractures are well connected. With decreasing matrix permeability, the histograms for the fractures and matrix become more separated, denoting the increasing influence of the fractures and transition to a true dual-porosity system. The velocity histograms for the fractures show a clear dependence on fracture aperture. In the variable fracture aperture case, four distinct peaks can be identified while only two are present in the uniform fracture aperture case. Also, the spread of the histogram is wider in the variable aperture case compared to the uniform aperture case. Both reflect stronger velocity variations in the variable aperture case compared to the uniform aperture due to the wider range of fracture permeabilities.

Figure 3 shows the concentration distributions for matrix permeabilities of $k_m = 10^{-11}$ m^2 (after 3 days), $k_m = 10^{-13}$ m^2 (after 90 days), and $k_m = 10^{-15}$ m^2 (after 90 days) for both fracture aperture cases. Note that the concentrations are already uniform after 90 days if the matrix permeability is $k_m = 10^{-11}$ m^2, because advective transport into and through the matrix blocks increases solute transfer between the fracture and the matrix. In all cases, solutes have broken through at the right model boundary in less than one day and the concentration distribution in the matrix is highly irregular. Generally, the

concentrations increase faster in smaller matrix blocks compared to larger matrix blocks, indicating a multi-rate solute exchange between fractures and matrix.

The $k_m = 10^{-11}$ m^2 case: Significant advective solute transport occurs in the matrix itself, hence the concentrations in the matrix increase faster closer to the inflow boundary (Figure 3a and d). Concentration gradients between the matrix and vertical fractures, i.e. fractures oriented perpendicular to the main flow direction, are smooth downstream of the fractures and steep upstream. Horizontal fractures partly show tapering in concentration gradients, i.e. the matrix concentration is higher upstream of fractures oriented sub-parallel to the main flow direction and lower downstream because exchange of solutes between fractures and matrix has occurred for a longer time upstream. All these are typical for an advective contribution to solute transport in the matrix. Concentration distributions for uniform fracture apertures show faster solute transport in the matrix because flow in the fractures is more homogeneous and hence solutes can enter the matrix more uniformly where they are transported downstream by advection.

The corresponding breakthrough curves at $\chi = 0.25$ and 0.5, and to a lesser extent at $\chi = 0.75$ (Figure 4a and d), show a characteristic slope change at early time. The lower part corresponds to the early breakthrough in the fractures and the higher to the breakthrough in the matrix. This slope change is less pronounced for the case of uniform fracture apertures because fractures with small apertures, which lead to increased advection in the matrix, are absent. The slope change becomes less evident with increasing breakthrough distance. This is because the mixing of the high-concentration and low-concentration fluids increases downstream and breakthrough concentrations become more uniform. Tailing, arising from the slow diffusive exchange of solute between the matrix

and fractures and slow transport in the matrix, is absent in all breakthrough curves, indicating that a true dual-porosity system is not present.

The $k_m = 10^{-13}$ m^2 case: Advective transport occurs predominantly in the fractures while solute transport in the matrix is dominated by diffusion (Figure 3b and e). Concentration levels in the matrix depend on the size of the individual blocks. Larger matrix blocks, where the concentration is still zero in the center, show that concentration gradients between matrix and perpendicular fractures are smoother downstream and steeper upstream, indicating minor contributions of advective transport in the matrix. Tapering is also not as prominent as in the $k_m = 10^{-11}$ m^2 case. The difference in concentration distributions for the variable and uniform fracture aperture cases decreases with decreasing matrix permeability (Figure 3) because solute advection in the matrix becomes less important.

Breakthrough curves exhibit significant tailing after one day (Figure 4b and e). This indicates that diffusive exchange between fractures and matrix and diffusion-dominated transport in the matrix dominates the transport behavior at "late time", indicative of a dual-porosity system, and occurs at variable rates because larger matrix blocks provide more storage for the solutes compared to smaller ones. Although the breakthrough curves for both fracture aperture cases show a similar qualitative behavior, a clear quantitative difference prevails. The variable fracture aperture case has a much more heterogeneous flow field in the fractures, which leads to more dispersive breakthrough curves with earlier arrivals.

The $k_m = 10^{-15}$ m^2 and $k_m = 10^{-17}$ m^2 cases: Advective transport in the matrix is negligible in theses cases (Figure 4c and f). Hence, results for both cases are almost

identical with only minor numerical variations in the breakthrough curves. Concentration gradients between fractures and matrix are steep even after 90 days. Matrix advection does not influence these gradients at all. Breakthrough curves show strong tailing and are identical for both these matrix permeabilities because even at $k_m = 10^{-15}$ m^2, the fractures already carry more than 3×10^5 times the flow than the rock matrix.

4. Continuous Time Random Walk Analysis

In this section, we briefly review the physics of the CTRW approach to transport; a more detailed analysis of the CTRW method can be found in Berkowitz et al. [2006]. CTRW generalizes the classical Random Walk approach to transport by introducing, in addition to the probability density functions (pdf) for the jump directions, $p(x)$, a retention-time pdf, $\psi(t)$. A CTRW characterized by $p(x)$ and $\psi(t)$ with finite first and second moments (e.g., $p(x) \sim N(0,1)$, and $\psi(t) = \exp(-t)$) is equivalent to the classical RW approach, and hence to an Fickian advective-dispersion formulation for transport. Many transport problems in heterogeneous porous materials can be characterized by a $\psi(t)$ for which the first temporal moment does not exists (or is very large), whereas the $p(x)$ can still be characterized by a Gaussian distribution [Cortis and Berkowitz, 2004; Cortis, 2007; Berkowitz et al., 2006].

In the continuum limit, the equation that governs CTRW transport reads:

$$\frac{\partial c(x,t)}{\partial t} = -\int_0^t M(t-t')\frac{\partial}{\partial x}\Big[c(x,t') - \alpha\frac{\partial c(x,t')}{\partial x}\Big]\,dt'. \tag{5}$$

Equation 5 is an partial integro-differential equation that states that the time variation of the solute concentration at a given point equal the time-convolution of the classical ADE

transport kernel, with a memory function $M(t)$ defined in term of the $\psi(t)$ as

$$M(t) = \frac{\bar{t}}{2\pi i} \int_{\Gamma} e^{ut} \frac{u \int_0^\infty e^{-ut}\psi(t)\,dt}{1 - \int_0^\infty e^{-ut}\psi(t)\,dt}\,du, \tag{6}$$

where Γ is a clockwise Hankel contour Krantz [1999], and $\bar{t}$ is a characteristic time. Note that Equation 5 was made non-dimensional using characteristic length, L, and time, $\bar{t}$, such that the non-dimensional transport velocity, $\bar{t}v/L = 1$. When $\psi(t) = \exp(-t)$, the memory function reduces to a Dirac delta, $M(t) = \delta(t)$, and Equation 5 reduces to the classical advection dispersion equation.

The correct estimation of the retention times distribution $\psi(t)$ is key for understanding the upscaled character of the solute transport. A number of functional forms for $\psi(t)$ have been proposed and applied to laboratory and field data, the most notable ones being the truncated power-law [Dentz et al., 2004] and the modified exponential [Cortis et al., 2004b]. These functional forms, however, have limited use in modeling extremely complex heterogeneity structures that involve non-trivial solute exchanges patterns between interconnected flow structures such as those found in more complex fracture networks [Cortis and Birkholzer, 2008].

The BTCs in Figure 4 do not exhibit a classical normal transport, and a careful analysis of the BTCs tails in double-logarithmic units does not reveal any significant power-law decay such as the -3/2 slope typical for matrix diffusion and rate-limited mass transfer [Haggerty et al., 2001]. Finding a suitable functional form for $\psi(t)$ is therefore a challenge. For this reason, in this study we use the non-parametric inversion algorithm (NPIA) first described by Cortis [2007]. The NPIA recovers a numerical approximation of the full spectrum of retention times, $\psi(t)$, without postulating its functional form a priori. An important finding made possible by the NPIA analysis of CTRW transport is that the

non-dimensional dispersivity coefficient, α, is not anymore a parameter associated with the microgeometry of the porous medium but rather an ancillary parameter associated with the particular distribution of retention times, $\psi(\tau|\alpha)$.

The coefficient α is the coefficient of variation of the spatial distribution of jump length, and as such, reflects the intimate connection between the distribution of jump length and durations, which characterizes the CTRW description of transport.

In other words, it is always possible to find a distribution of retention times for any reasonably small value of α close to the small-scale dispersion estimate. In this study the longitudinal and transverse dispersivities were set to $\alpha_L = 0.01$ m and $\alpha_T = 0.001$ m, respectively, and the value of α/L in equation Equation 5 was taken to be roughly 100 times larger, i.e., $\alpha/L = 5 \times 10^{-2}$. The reason for this choice is that using $\alpha \sim \alpha_L$ makes the character of the ADE almost hyperbolic rather parabolic and requires different numerical solution schemes. The advantage of the NPIA approach with respect to other upscaling methods is therefore in the reduction of the dispersivity to a scale-independent coefficient.

Figures 5 and 6, show the CTRW-NPIA best-fit results for the constant and variable fracture aperture cases, respectively. The left-hand panels show the numerical computations (black dots) for the four sections $\chi = 0.25, 0.5, 0.75, 0.99$, for each of the four matrix-fracture permeability contrasts. The solid blue line on top of the $\chi = 0.5$ breakthrough curves represents the NPIA best fit. The corresponding $\psi(t)$ is shown as blue dots on the right-hand side of each figure. The dashed black line is the exponential $\exp(-t)$, for reference. Having this estimated $\psi(t)$ calibrated on the $\chi = 0.5$ section, we can now predict the breakthrough curves at $\chi = 0.75, 0.99$, and make a backwards prediction for

the BTC at $\chi = 0.25$ (red solid lines). We find a perfect agreement between the CTRW predictions and the direct numerical simulations for all the four matrix-fracture permeability contrast cases, both for the constant and variable aperture cases. Calibration of the $\psi(t)$ on the BTC at $\chi = 0.25$ (not shown) yields identical results to the one presented in Figure 5.

We must stress that the NPIA yields only a numerical approximation of the distribution of retention times (blue dots), and not an explicit functional form. It is nonetheless possible to gain valuable insight by carefully analyzing the fine details of the best-fit $\psi(\tau|\alpha)$.

In the case of constant fracture aperture, for instance, the best-fit $\psi(t)$ does not exhibit power-law like decay for any significantly long time period; as a consequence, the system cannot be modeled neither by (truncated) power-law expressions, nor by means of any fractional derivatives approach. The plot in Figure 5 suggest, however, that the best-fit $\psi(\tau|\alpha)$ can be decomposed into the sum of three exponentials each for all the various matrix permeability cases analyzed in this study:

$$\psi(\tau|\alpha) = \frac{1}{\sum_{i=1}^{3} \frac{a_i}{b_i}} \sum_{i=1}^{3} a_i \exp(-b_i \tau), \tag{7}$$

where the coefficients $a_i > 0$, and $b_i > 0$ are listed in Table 3. We recall here that a decaying exponential is the signature of "normal" (Gaussian) transport.

The exponential component with the largest decay rate value, b_1, (cyan dashed line) may be interpreted as the contribution to transport from the fractures, whereas the component with the smallest value, b_3, (red dashed line) may be interpreted as the contribution due to the flow in the matrix. The intermediate value, b_2, (green dashed line), may be interpreted as the contribution to transport arising from the continuous exchange between

matrix and fractures. We have therefore reduced the numerical approximation of the $\psi(t)$ to a functional form depending on a (relatively small) number of parameters, i.e., the coefficients of the exponential components, in addition to the (arbitrarily fixed) value of the dispersivity, α.

For the case with variable fracture aperture, however, it is not possible to decompose the best-fit $\psi(t)$ in the sum of three exponentials. Despite the general qualitative agreement between the $\psi(t)$ and the best-fit sum-of-exponentials decomposition, it is clear that the individual segments of the $\psi(t)$ which we have associated to fracture, matrix, and exchange transport, respectively, cannot be assimilated, in this case, to decaying exponentials. The three regions of the distribution, more closely resemble algebraic decaying curves (power-laws), the parameters of which, given the relatively short time span, are difficult to estimate. This can be readily understood in the context of the CTRW framework, by noting that the disorder associated with any given attribute of the heterogeneity give raise in most cases to algebraic decays in the distribution of retention times. In this case, it is the heterogeneity in the distribution of fracture apertures, and the subsequently stronger variations in fracture velocities (Figure 2), which is responsible for the algebraic decay characterizing the $\psi(t)$.

The CTRW-NPIA analysis of complex fracture-matrix transport problems presented in this work has proved to be a very effective and flexible tool for the determination of various flow regimes, and for discriminating between systems with constant or variable fracture aperture. A more systematic analysis of the dependence of the coefficients of the exponential components of ψ on fracture density and permeability contrast is needed and will be the object of a future study.

Moreover, the question of how much heterogeneity needs to be seen by the tracer to have a correct estimate of the $\psi(t)$ is an open one. Preliminary computations have shown that, for the system analyzed in this study, it is sufficient to calibrate the $\psi(t)$ on a BTC at $\chi = 0.1$. For other less regular and poorly connected fracture systems, however, the calibration of the $\psi(t)$ does not seem to yield good results for $\chi < 0.25$. These important questions will be analyzed in a separate study.

5. Concluding remarks

We have carried out high-resolution simulations of solute transport in real fracture-matrix geometries and for several combinations of fracture and matrix permeabilities, representing a wide range of highly heterogeneous fracture-matrix transport systems where transport velocities can varies over 10 orders of magnitude. We used these simulations to generate a suite of surrogate breakthrough curves, all of which show the early breakthrough and long tailing typical of anomalous transport. We then extracted the residence time distribution $\psi(t)$ with the non-parametric CTRW method.

The non-parametric CTRW method faithfully predicts the anomalous transport behaviour in these realistic representations of complexly and naturally fractured porous media. It accurately captures the various forms of early breakthrough and long tailing observed in our simulations, for cases where diffusion in the matrix dominates to cases with advective transport contributions in the matrix. The resulting $\psi(t)$ could be used to in new, CTRW-based, upscaling approaches, to adequately simulate fractured reservoirs at the field-scale [Rhodes et al., 2008, 2009].

The $\psi(t)$ differs significantly from a decaying exponential $\exp(-t)$, which represents the classical advection-diffusion equation with a macro dispersivity. If the fracture aperture is

uniform, $\psi(t)$ can be decomposed into the sum of three exponentials contributions. Each has a clear physical meaning associated with transport in fractures, matrix, and their interaction, respectively. For the case of variable fracture aperture, however, it is not possible to obtain such a simple decomposition, and the portion of $\psi(t)$ corresponding to the aforementioned fracture, matrix, and exchange terms, resemble more closely power-laws than exponentials. This difference represents an attractive feature of our model, because the success or failure in obtaining such a decomposition allows ultimately to discriminate between systems with relatively constant and variable fracture apertures.

Future work will focus on the ergodicity of the system, i.e., we will investigate the question of how much heterogeneity a tracer must encounter before a reliable $\psi(t)$ can be extracted. Preliminary studies for the "Bristol Channel" fracture network which is the object of this work indicate that the breakthrough curve can be calibrated successfully at $\chi = 0.1$, i.e., when the tracer has encountered just 10% of the heterogeneity. For other systems, however, such length depends on the stationarity of the heterogeneity field.

Acknowledgments. S. Geiger thanks the Edinburgh Collaborative of Subsurface Science and Engineering, a joint research institute of the Edinburgh Research Partnership in Mathematics and Engineering, for financial support. We are grateful to Klaus Stüben for providing us with a free version of the SAMG solver and to Mandefro Belayneh for making the Bristol Channel fracture patterns available to us. This work was supported, in part, by the U.S. Department of Energy under Contract No. DE-AC02-05CH11231. We thank S. Finsterle for interesting scientific discussions and constructive criticism. The

manuscript benefitted from the constructive comments of three anonymous reviewer and the associate editor.

References

A. Assteerawatt. *Flow and transport modelling of fractured aquifers based on a geostatistical approach.* PhD thesis, Institut für Wasserbau, Universität Stuttgart, Germany, 2008.

G. E. Barenblatt, I. P. Zheltov, and I. N. Kochina. Basic concepts in the theory of seepage of homogeneous liquids in fissured rocks. *Journal of Applied Mathematics (USSR)*, 24: 1286–1303, 1960.

M. Belayneh. Paleostress orientation inferred from surface morphology of joints on the southern margin of the bristol channel basin, uk. In J. W. Cosgrove and T. Engelder, editors, *The Initiation, Propagation, and Arrest of Joints and Other Fractures*, volume 231 of *Geological Society of London Special Publications*, pages 243–255. 2004.

M. Belayneh, S. Geiger, and S. K. Matthäi. Numerical simulation of water injection into layered fractured carbonate reservoir analogs. *AAPG Bulletin*, 90(10):1473–1493, 2006.

R. Benke and S. Painter. Modeling conservative tracer transport in fracture networks with a hybrid approach based on the Boltzmann transport equation. *Water Resources Research*, 39(11):1324, 2003. doi: doi:10.1029/2003WR001966.

B. Berkowitz. Characterizing flow and transport in fractured geological media: A review. *Advances in Water Resources*, 25(8-12):861–884, 2002.

B. Berkowitz and H. Scher. On characterization of anomalous dispersion in porous and fractured media. *Water Resources Research*, 31(6):1461–1466, 1995.

B. Berkowitz and H. Scher. Anomalous transport in random fracture networks. *Physical Review Letters*, 20:4038–4041, 1997.

B. Berkowitz and H. Scher. Theory of anomalous transport in random fracture networks. *Physical Review E*, 57(5):5858–5869, 1998.

B. Berkowitz, G. Kosakowski, G. Margolin, and H. Scher. Application of continuous time random walk theory to tracer test measurements in fractured and heterogeneous porous media. *Ground Water*, 39(4):593–604, 2001.

B. Berkowitz, A. Cortis, M. Dentz, and H. Scher. Modeling non-fickian transport in geological formations as a continuous time random walk. *Reviews of Geophysics*, 44(2): 49, 2006.

B. Berkowitz, S. Emmanuel, and H. Scher. Non-fickian transport and multiple-rate mass transfer in porous media. *Water Resources Research*, 44(3):W03402, 2008. doi: doi:10.1029/2007WR005906.

R. Bibby. Mass transport of solutes in dual-porosity media. *Water Resources Research*, 17(4):1075–1081, 1981.

B. Bijeljic and M. J. Blunt. Pore-scale modeling and continuous time random walk analysis of dispersion in porous media. *Water Resources Research*, 42(1), 2006.

B. Bijeljic, A. H. Muggeridge, and M. J. Blunt. Pore-scale modeling of longitudinal dispersion. *Water Resources Research*, 40(11), 2004.

J. Birkholzer and G. Rouve. Dual-continuum modeling of contaminant transport in fractured formations. In *X International Conference on Computational Methods in Water Resources, Heidelberg, Germany*, 1994.

E. Bonnet, O. Bour, N. E. Odling, P. Davy, I. Main, P. Cowie, and B Berkowitz. Scaling of fracture systems in geological media. *Reviews of Geophysics*, 39(3):347–383, 2001.

A. Cortis. Peclet-dependent memory kernes for transport in heterogeneous media. *Physical Review E*, 76:030102(R), 2007.

A. Cortis and B Berkowitz. Anomalous transport in "classical" soil and sand columns. *Soil Science Society of America Journal*, 68:1539–1548, 2004.

A. Cortis, H. Gallo, H. Scher, and B Berkowitz. Numerical simulation of non-fickian transport in geological formations with multiple-scale heterogeneities. *Water Resources Research*, 40:W04209, 2004. doi: 10.1029/2003WR002750.

A. Cortis, Y. Chen, H. Scher, and B Berkowitz. Quantitative characterization of pore-scale disorder on transport in "homogeneous" granular media. *Physical Review E*, 70: :041108, 2004.

A. Cortis and B Berkowitz. Computing the full time evolution of anomalous breakthrough curves:The CTRW Matlab toolbox. *Ground Water*, 43:(6) 947–950, 2005.

A. Cortis, T. Harter, L. Hou, E . R. Atwill, A. Packman, and P. Green. Transport of cryptosporidium parvum in porous media: Long-term elution expierments and continuous time random walk foltration modeling. *Water Resources Research*, 42:WS12S13, 2006. doi: 10.1029/2006WR004897.

A. Cortis and T. A. Ghezzehei. On the transport if emulsions in porous media. *Journal of Colloids and Interface Science*, 313(1):1–4, 2007.

A. Cortis and J. Birkholzer. Continuous time random walk analysis of solute transport in fractured porous media. *Water Resources Research*, 44:W06414, 2008. doi: 10.1029/2007WR006569.

M. Dentz and B. Berkowitz. Transport behavior of a passive solute in continuous time random walks and multirate mass transfer. *Water Resources Research*, 39(5):1111, 2003. doi: 10.1029/2001WR001163.

M. Dentz, A. Cortis, H. Scher, and B. Berkowitz. Time behaviour of solute transport in heterogeneous media: Transition from anomalous to normal transport. *Advances in Water Resources*, 27(2):155-173, 2004.

G. Di Donato, E. O. Obi, and M. J. Blunt. Anomalous transport in heterogeneous media demonstrated by streamline-based simulation. *Geophysical Research Letters*, 30(12): 1608, 2003. doi: 10.1029/2003GL017196.

R. C. Dykhuizen. A new coupling term for dual-porosity models. *Water Resources Research*, 26(2):351–356, 1990.

S. Emmanuel and B. Berkowitz. Continuous time random walks and heat transfer in porous media. *Transport in Porous Media*, 67(3):413–430, 2007.

C. E. Feehley, C. Zheng, and F. J. Mozl. A dual-domain mass trasfer approach for modeling solute transport in heterogeneous aquifers: Application to the macrodisperiojn experiment (made) site. *Water Resources Research*, 36(9):2501–2515, 2000.

G. P. Flach, S. A. Crisman, and F. J. Molz. Comparison between single-domain and dual-domain subsurface transport models. *Groundwater*, 42(6):815–828, 2004.

S. Geiger and S. Emmanuel. Non-fourier thermal transport in fractured geological media. *Water Resources Research*, 2010, doi:10.1029/2009WR008671.

S. Geiger, S. G. Roberts, S. K. Matthäi, C. Zoppou, and A. Burri. Combining finite element and finite volume methods for efficient multiphase flow simulations in highly heterogeneous and structurally complex geologic media. *Geofluids*, 4(4):284–299, 2004.

S. Geiger, S. Matthäi, J. Niessner, and R. Helmig. Black-oil simulations for three-component - three-phase flow in fractured porous media. *SPE Journal*, 14(2):338–354, 2009.

R. Haggerty and S. M. Gorelick. Multiple-mass transfer for modeling diffusion and surface reactions in media with pore-scale heterogeneities. *Water Resources Research*, 31(10): 2383–2400, 1995.

R. Haggerty, S. A. McKenna, L. C. Meigs. On the late-time behavior of tracer test breakthrough curves. *Water Resources Research*, 36(12):3467–3479, 2000.

R. Haggerty, S. W. Fleming, L. C. Meigs, and S. A. McKenna. Tracer tests in a fractured dolomite 2. Analysis of mass transfer in single-well injection withdrawal test. *Water Resources Research*, 37(5):1129–1142, 2001.

H. Haegland, A. Assteerawatt, H. K. Dahle, G. T. Eigestat, and R. Helmig. Comparison of cell- and vertex-centered discretization methods for flow in a two-dimensional discrete-fracturematrix system. *Advances in Water Resources*, 32:1740–1755, 2009.

H. Hoteit and A. Firoozabadi. Multicomponent fluid flow by discontinuous galerkin and mixed methods in unfractured and fractured media. *Water Resources Research*, 41: W11412, 2005. doi: 10.1029/2005WR004339.

H. Hoteit and A. Firoozabadi. Numerical modeling of two-phase flow in heterogeneous permeable media with different capillarity pressures. *Advances in Water Resources*, 31 (1):56–73, 2008a.

H. Hoteit and A. Firoozabadi. An efficient numerical model for incompressible two-phase flow in fractured media. *Advances in Water Resources*, 31(6):891–905, 2008b.

P. S. Huyakorn, B. H. Lester, and C. R. Faust. Finite element techniques for modeling groundwater flow in fractured aquifers. *Water Resources Research*, 19(4):1019–1035, 1983a.

P. S. Huyakorn, B. H. Lester, and J. W. Mercer. An efficient finite element technique for modeling transport in fractured porous media: 1. single species transport. *Water Resources Research*, 19(3):8410854, 1983b.

P. S. Huyakorn, B. H. Lester, and J. W. Mercer. An efficient finite element technique for modeling transport in fractured porous media: 2. nuclide decay chain transport. *Water Resources Research*, 19(5):1286–1296, 1983c.

R. Juanes, J. Samper, and J. Molinero. A general and efficient formulation of fractures and boundary conditions in the finite element method. *International Journal for Numerical Methods in Engineering*, 54(12):1751–1774, 2002.

M. Karimi-Fard and A. Firoozabadi. Numerical simulation of water injection in fractured media using the discrete-fracture model and the galerkin method. *SPE Reservoir Evaluation & Engineering*, 6(2):117–126, 2003.

M. Karimi-Fard, L. J. Durlofsky, and K. Aziz. An efficient discrete-fracture model applicable for general-purpose reservoir simulators. *SPE Journal*, 9(2):227–236, 2004.

J. G. Kim and M. D. Deo. Finite element, discrete-fracture model for multiphase flow in porous media. *AIChE Journal*, 46(6):1120–1130, 2000.

G. Kosakowski, B. Berkowitz, and H. Scher. Analysis of field observations of tracer transport in a fractured till. *Journal of Contaminant Hydrology*, 47:29–51, 2001.

S. G. Krantz. Handbook of Complex Variables, Boston, MA: Birkhäuser, 1999.

P. C. Lichtner and Q. Kang. Upscaling pore-scale reactive transport equations using a multiscale continuum formulation *Water Resources Research*, 43, WS12S15, 2007. doi: 10.1029/2006WR005664.

S. K. Matthäi and M. Belayneh. Fluid flow partitioning between fractures and a permeable rock matrix. *Geophysical Research Letters*, 31(7):L07602, 2004.

S. K. Matthäi, A. Mezentsev, and M. Belayneh. Finite element-node-centered finite-volume two-phase-flow experiments with fractured rock represented by unstructured hybrid-element meshes. *SPE Reservoir Evaluation & Engineering*, 10(6):740–756, 2007.

S. K. Matthäi, H. M. Nick, C. Pain, and I. Neuweiler. Simulation of solute transport through fractured rock: A higher-order accurate finite-element finite-volume method permitting large time steps. *Transport in Porous Media*, 2010, 83(2):289–318, doi: DOI 10.1007/s11242-009-9440-z.

C. I. McDermott, R. Walsh, R. Mettier, G. Kosakowski, and O. Kolditz. Hybrid analytical and finite element numerical modeling of mass and heat transport in fractured rocks with matrix diffusion. *Computational Geosciences*, 13:349–361, 2009.

S. A. McKenna, L. C. Meigs, and R. Haggerty. Tracer tests in a fractured dolomite 3. Double-porosity, multi-rate mass transfer processes in convergent flow tracer tests. *Water Resources Research*, 37(5):1143–1154, 2001.

J. E. P. Monteagudo and A. Firoozabadi. Control-volume method for numerical simulation of two-phase immiscible flow in two- and three-dimensional discrete-fractured media. *Water Resources Research*, 40(7):W07405, 2004. doi: 10.1029/2003WR002996.

J. Niessner, R. Helmig, H. Jakobs, and J. E. Roberts. Interface condition and linearization schemes in the newton iterations for two-phase flow in heterogeneous porous media.

Advances in Water Resources, 28(7):671–687, 2005.

B. Noetinger and T. Estebenet. Up-scaling of double porosity fractured media using continuous-time random walks methods. *Transport in Porous Media*, 39:315-337, 2000.

B. Noetinger, T. Estebenet, and P. Landereau. A direct determination of the transient exchange term of fractured media using a continuous time random walk method. *Transport in Porous Media*, 44:539-557, 2001a.

B. Noetinger, T. Estebenet, and M. Quintard. Up-scaling flow in fractured media: Equivalence between the large scale averaging theory and the continuous time random walk method. *Transport in Porous Media*, 43:581-596, 2001b.

S. Painter and V. Cvetkovic. Upscaling discrete fracture network simulations: An alternative to continuum transport models. *Water Resources Research*, 41, W02002, 2005. doi: doi:10.1029/2004WR003682.

A. Paluszny, S. K. Matthäi, and M. Hohmeyer. Hybrid finite element-finite volume discretization of complex geologic structures and a new simulation workflow demonstrated on fractured rocks. *Geofluids*, 7(2):186–208, 2007.

V. Reichenberger, H. Jakobs, P. Bastian, and R. Helmig. A mixed-dimensional finite volume method for two-phase flow in fractured porous media. *Advances in Water Resources*, 29(7):1020–1036, 2006.

M. E. Rhodes, B. Bijeljic, and M. J. Blunt. Pore-to-field simulation of single-phase transport using continuous time random walks. *Advances in Water Resources*, 31(12):1527–1539, 2008.

M. E. Rhodes, B. Bijeljic, and M. J. Blunt. A rigorous pore- to field-scale simulation method for single-phase flow based on continuous-time random walks. *SPE Journal*, 14

(1):88–94, 2009.

H. Scher and M. Lax. Stochastic transport in a disordered solid. ii. impurity and conduction. *Physical Review B*, 7:4502–4519, 1973a.

H. Scher and M. Lax. Stochastic transport in a disordered solid. i. theory. *Physical Review B*, 7:4491-4502, 1973b.

K. Stüben. A review of algebraic multigrid. *Journal of Computational an Applied Mathematics*, 128:281–309, 2001.

K. Stüben and T. Clees. Samg user's manual. release 22c. Technical report, Fraunhofer Institute for Algorithms and Scientific Computing., 2005.

J. E. Warren and P. J. Root. The behavior of naturally fractured reservoirs. *SPE Journal*, 3(3):244–255, 1963.

R. W. Zimmerman, G. S. Bodvarsson, and E. M. Kwicklis. Adsorption of water into porous blocks of various shapes and sizes. *Water Resources Research*, 26(11):2797–2806, 1990.

R. W. Zimmerman, G. Chen, T. Hadgu, and Bodvarsson G. S. A numerical dual-porosity model with semianalytical treatment of fracture/matrix flow. *Water Resources Research*, 29(7):2127–2137, 1993.

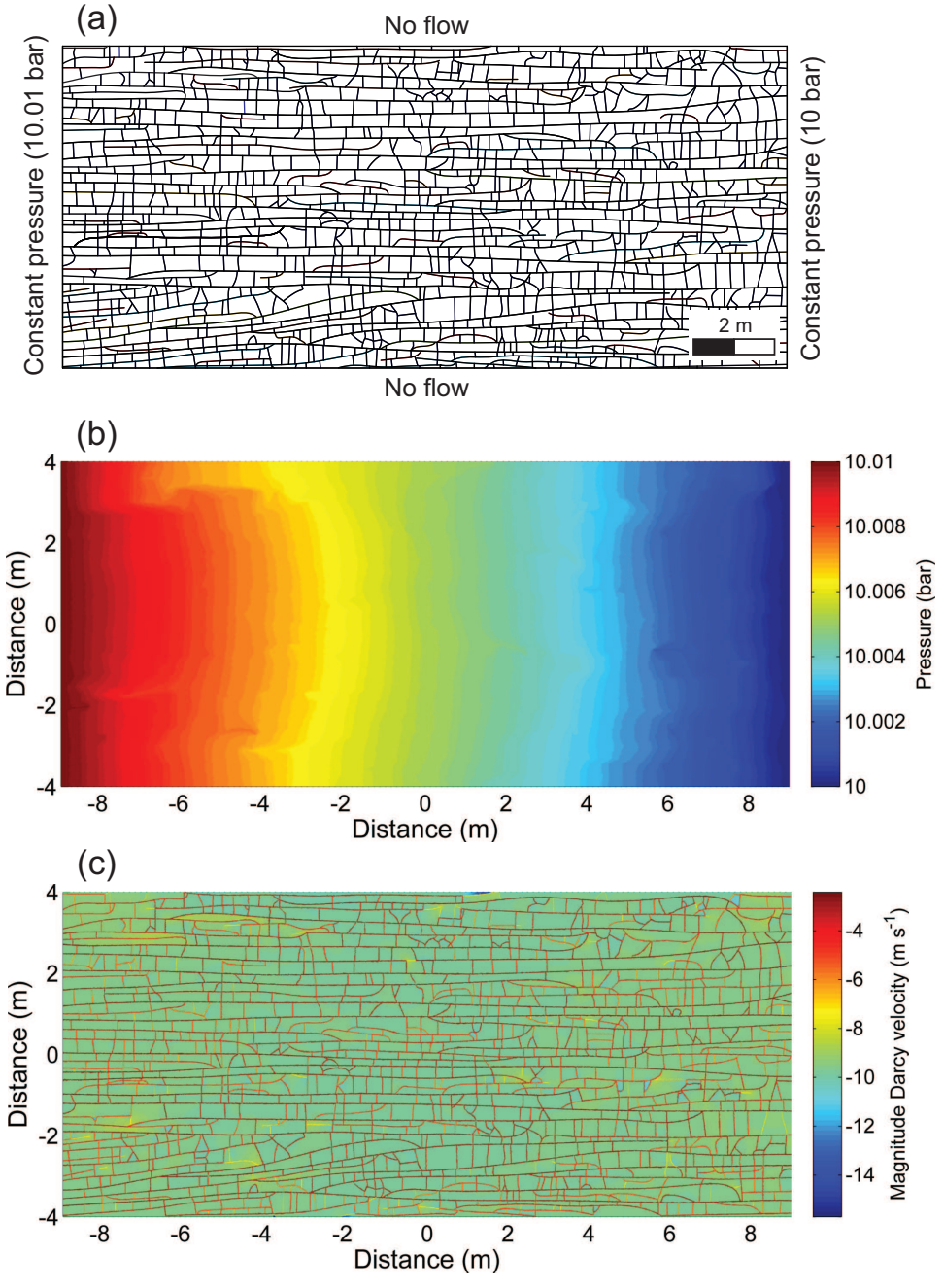

Figure 1. Fracture geometry of the Bristol Channel fractured reservoir analogue (a), fluid pressure distribution for a matrix permeability of $k_m = 10^{-15}$ m^2 (b), and logarithm of the magnitude of the Darcy velocity (c). Fracture apertures vary between 0.1 and 1.2

Parameter	Symbol	Value	Unit
Matrix			
Permeability	k_m	case dependent†	m^2
Porosity	φ_m	0.25	–
Longitudinal dispersion	α_L	0.01	m
Transversal dispersion	α_T	0.001	m
Diffusivity	D	10^{-9}	$m^2\ s^{-1}$
Fractures			
Permeability	k_f	variable‡	m^2
Porosity	φ_f	1.0	–
Longitudinal dispersion	α_L	0.01	m
Transversal dispersion	α_T	0.001	m
Diffusivity	D	10^{-9}	$m^2\ s^{-1}$
Initial conditions			
Viscosity	μ	0.001	Pa s
Concentration	c	0.0	$kg\ m^{-3}$
Pressure	p	variable*	bar
Boundary conditions			
Inflow concentration	$c_{x=0}$	1.0	$kg\ m^{-3}$
Outflow concentration	$c_{x=x_{max}}$	$\partial c/\partial x = 0$	–
Inflow pressure	$p_{x=0}$	10.01	bar
Outflow pressure	$p_{x=x_{max}}$	10	bar

Table 1. Model parameters and initial and boundary conditions. † Matrix permeability is constant and uniform at 10^{-11}, 10^{-13}, 10^{-15}, or 10^{-17} m^2. ‡ Fracture permeability is computed from the parallel plate law as $k_f = a^2/12$. The fracture aperture a either varies from 0.1 to 1.2 mm in individual fractures or is uniform at 1 mm. * See Figure 1b for the pressure field.

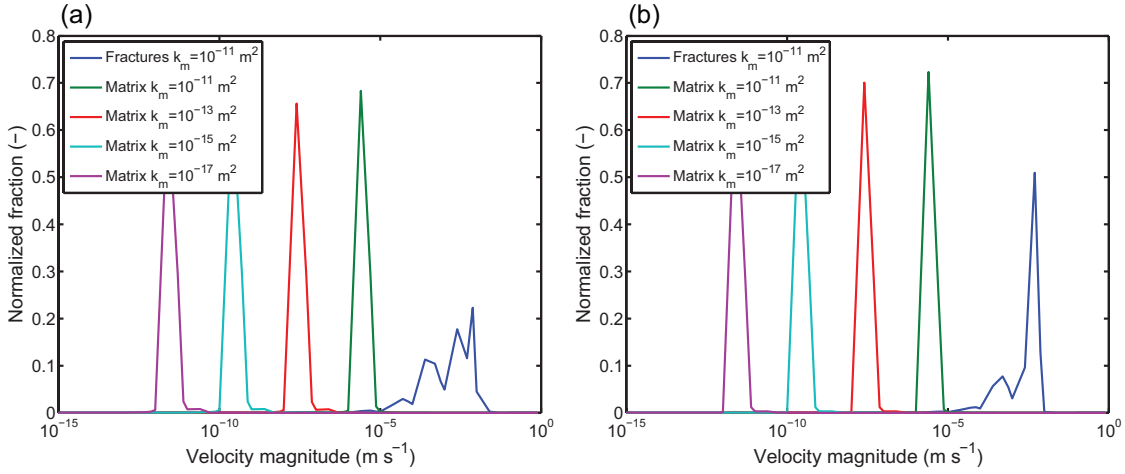

Figure 2. Velocity histograms for the variable fracture aperture (a) and uniform fracture aperture (b) case. Note that the velocity distributions in the fractures are almost completely insensitive to changes in matrix permeability and hence only the velocity histograms for the fractures for the $k_m = 10^{-11}$ m^2 case are shown.

Table 2. Averaged horizontal transport properties for the four different matrix permeabilities k_m of the model "Bristol Channel". Note that the average porosity $\hat{\phi}$ is constant at $\hat{\phi} = 0.254$ in all four cases.

k_m (m^2)	$\hat{k}$ (m^2)	$\hat{v}$ (m s^{-1})	R (–)
Variable fracture aperture, k_f between 0.1 and 1.2 mm			
10^{-11}	3.26×10^{-10}	1.81×10^{-5}	31.76
10^{-13}	3.11×10^{-10}	1.73×10^{-5}	3134
10^{-15}	3.11×10^{-10}	1.73×10^{-5}	3.13×10^{5}
10^{-17}	3.11×10^{-10}	1.73×10^{-5}	3.13×10^{7}
Constant fracture aperture, $k_f = 1$ mm			
10^{-11}	3.35×10^{-10}	1.86×10^{-5}	32.75
10^{-13}	3.22×10^{-10}	1.79×10^{-5}	3238
10^{-15}	3.22×10^{-10}	1.79×10^{-5}	3.24×10^{5}
10^{-17}	3.22×10^{-10}	1.79×10^{-5}	3.24×10^{7}

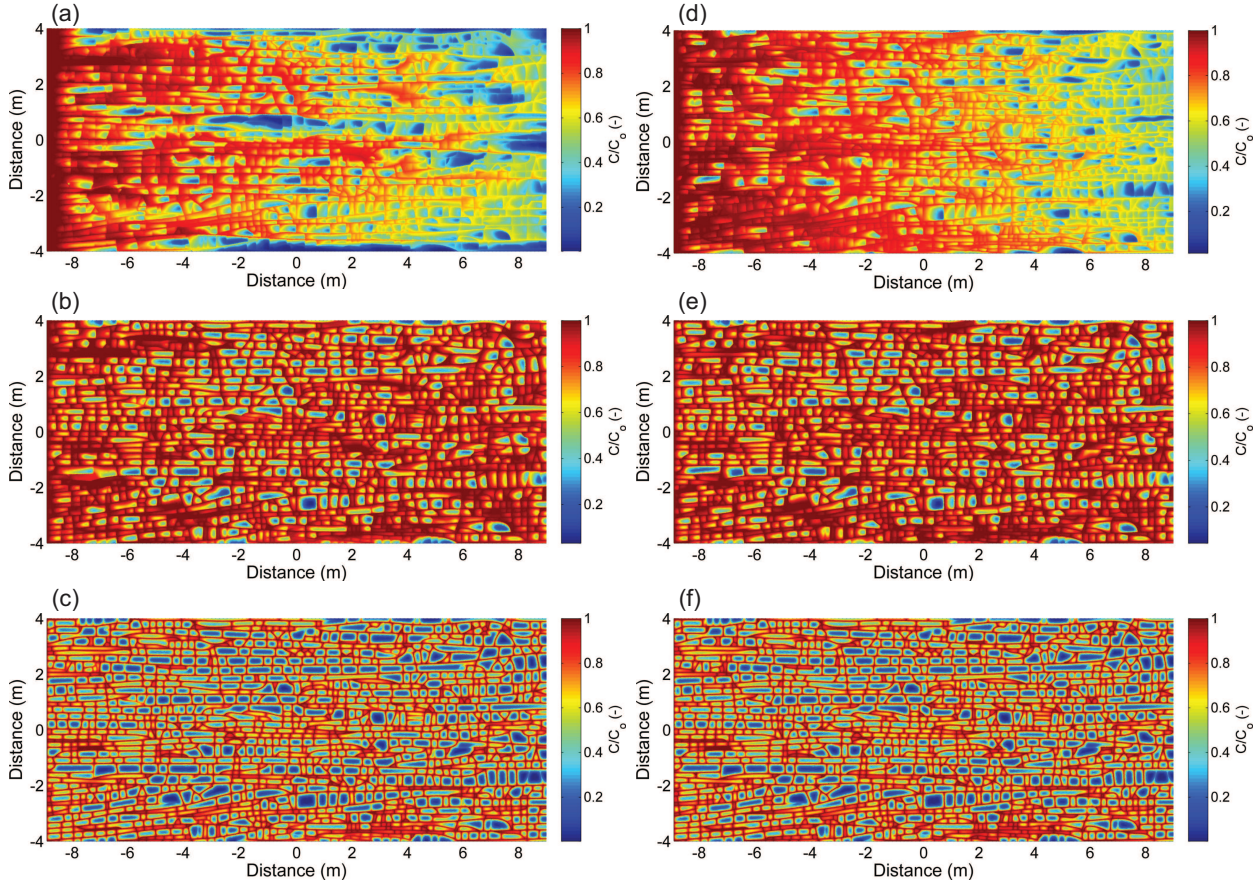

Figure 3. Concentration distributions for $k_m = 10^{-11}$ m^2 after 3 days (a, d), for $k_m = 10^{-13}$ m^2 after 90 days (b, e), and for $k_m = 10^{-15}$ m^2 after 90 days (c, f). Fracture apertures vary between 0.1 and 1.2 mm (a to c) or are uniform at 1 mm (d to f). The concentration distributions for $k_m = 10^{-15}$ and $k_m = 10^{-17}$ are essentially identical for both fracture aperture cases.

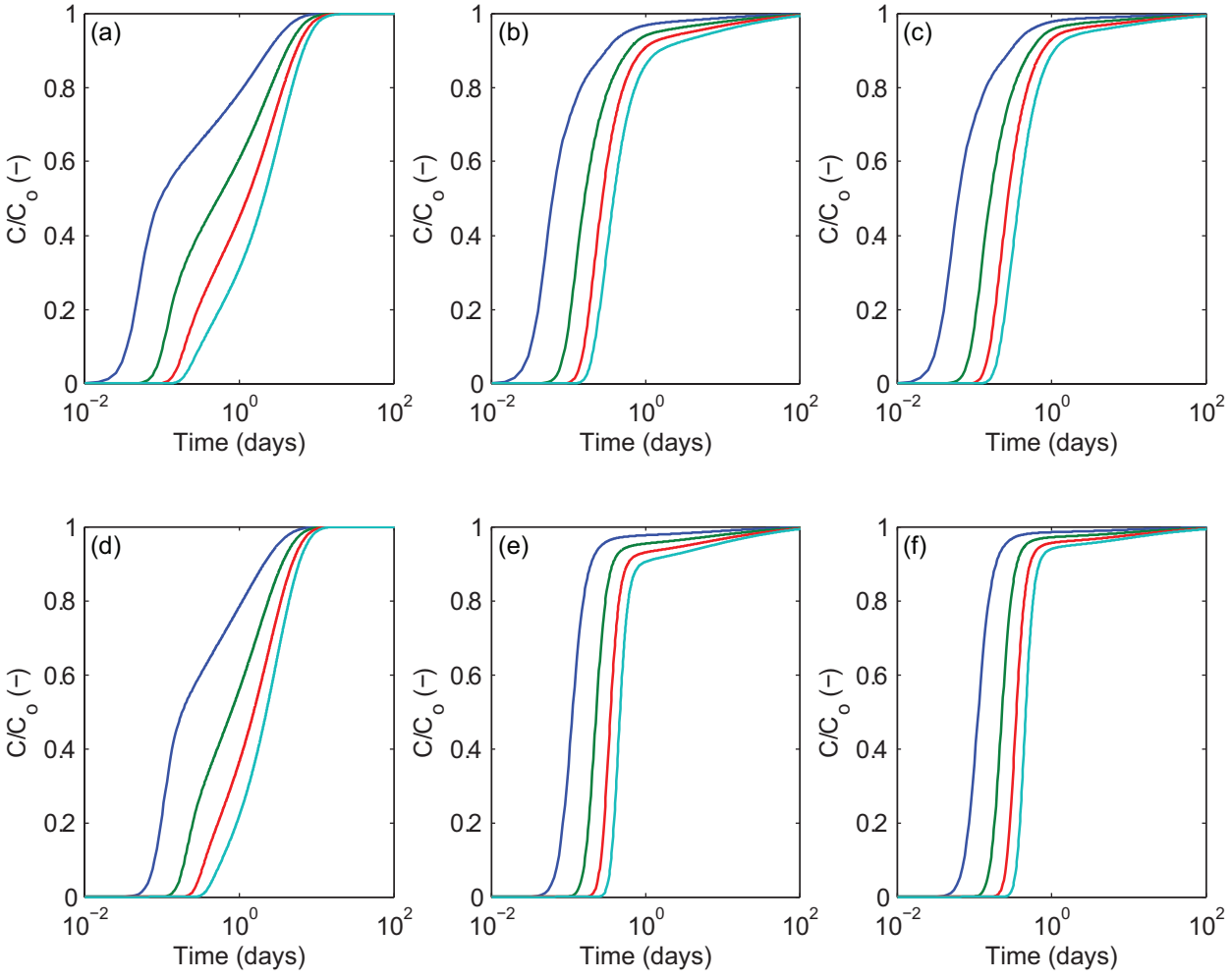

Figure 4. Breakthrough curves for $k_m = 10^{-11}$ m^2 (a, d), $k_m = 10^{-13}$ m^2 (b, e), and $k_m = 10^{-15}$ m^2 (c, f) measured at different distances, denoted as $\chi = x/L$, away from the left (inflow) model boundary. Fracture apertures vary between 0.1 and 1.2 mm (a to c) or are uniform at 1 mm (d to f). The blue line corresponds to $\chi = 0.25$, the green line to $\chi = 0.5$, the red line to $\chi = 0.75$, and the cyan line to $\chi = 0.999$. The breakthrough curves for $k_m = 10^{-15}$ and $k_m = 10^{-17}$ are essentially identical for both fracture aperture cases.

Table 3. Decomposition of the non-parametric best-fit $\psi(t)$ in the sum of 3 decaying exponentials (normal modes of transport). Coefficients a_i, and b_i, are the amplitude and decay rate, respectively, for the expression in Equation 7.

k_m (m^2)	a_1	a_2	a_3	b_1	b_2	b_3
Variable fracture aperture, k_f between 0.1 and 1.2 mm						
10^{-11}	8.21	4.81×10^{-3}	3.73×10^{-1}	24.25	1.06	5.85×10^{-1}
10^{-13}	7.64	1.29×10^{-1}	4.96×10^{-3}	9.16	1.19	8.52×10^{-2}
10^{-15}	8.13	7.12×10^{-1}	4.07×10^{-3}	11.47	2.87	9.30×10^{-2}
10^{-17}	8.29	8.65×10^{-1}	4.13×10^{-3}	12.32	3.05	9.41×10^{-2}
Constant fracture aperture, $k_f = 1$ mm						
10^{-11}	4.57	1.83×10^{-2}	5.82×10^{-1}	20.36	4.46	7.55×10^{-1}
10^{-13}	6.05	4.03×10^{-2}	8.67×10^{-3}	6.67	9.86×10^{-1}	1.69×10^{-1}
10^{-15}	6.05	1.64×10^{-2}	6.00×10^{-3}	6.38	9.54×10^{-1}	1.75×10^{-1}
10^{-17}	6.05	1.58×10^{-2}	5.67×10^{-3}	6.37	9.09×10^{-1}	1.68×10^{-1}

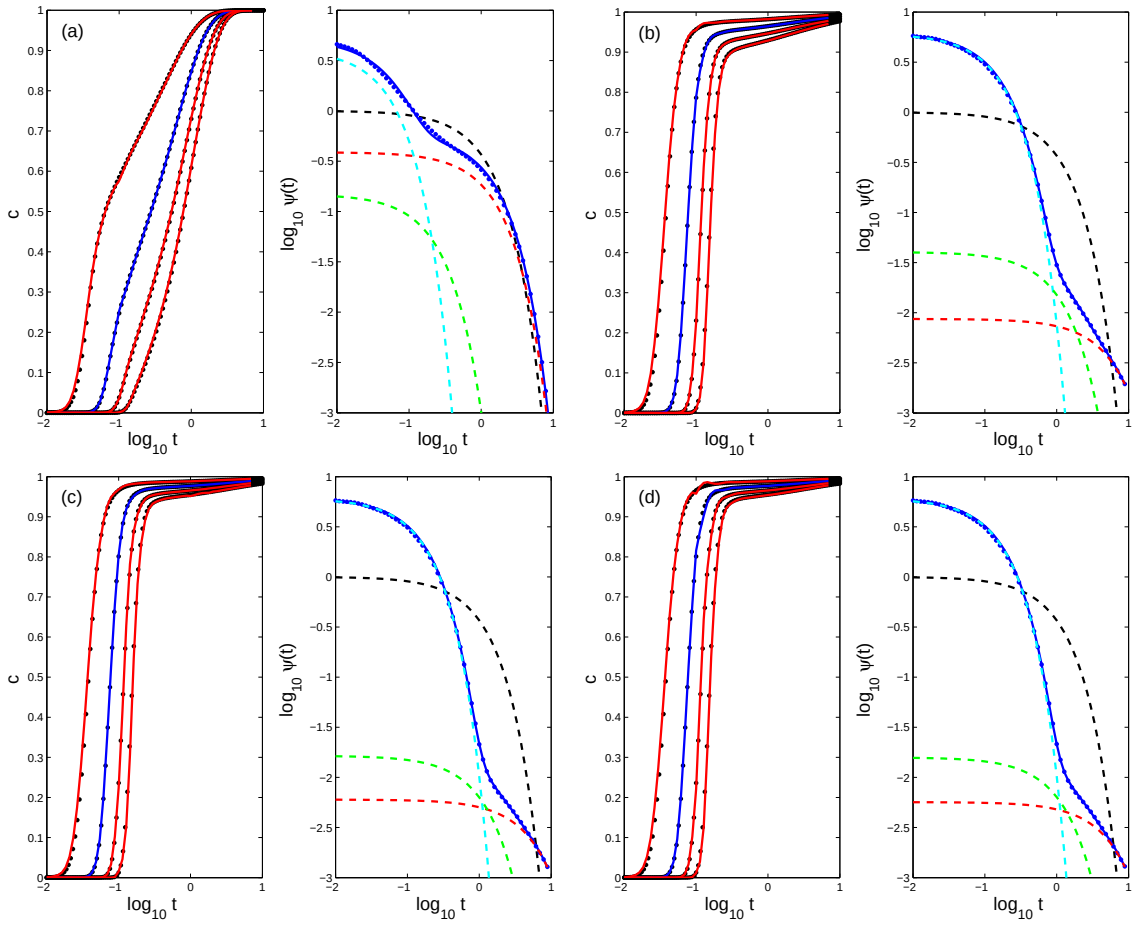

Figure 5. Left-hand side panels of (a)-(d): Breakthrough curves for $k_m = 10^{-11}$ m^2 (a), $k_m = 10^{-13}$ m^2 (b), $k_m = 10^{-15}$ m^2 (c), and $k_m = 10^{-17}$ m^2 (d) measured at different distances, denoted as $\chi = x/L$, away from the left (inflow) model boundary. The fracture apertures are constant at 1 mm. The time scale is non-dimensional. Black dots represent numerical computations, solid blue line ($\chi = 0.5$) is the NPIA-CTRW best-fit, and solid red lines are the predictions based on the calibrated $\psi(t)$. Right-hand size of (a)-(d): distribution of retention time, $\psi(t)$. calibrated on the BTC measured at $\chi = 0.5$. The dashed black line is the ADE decaying exponential, $\exp(-t)$. The solid blue line represents the sum of three individual decaying exponentials shown as light-blue, green, and red dashed lines, respectively. The coefficients of the decaying exponential are reported in Table 3.

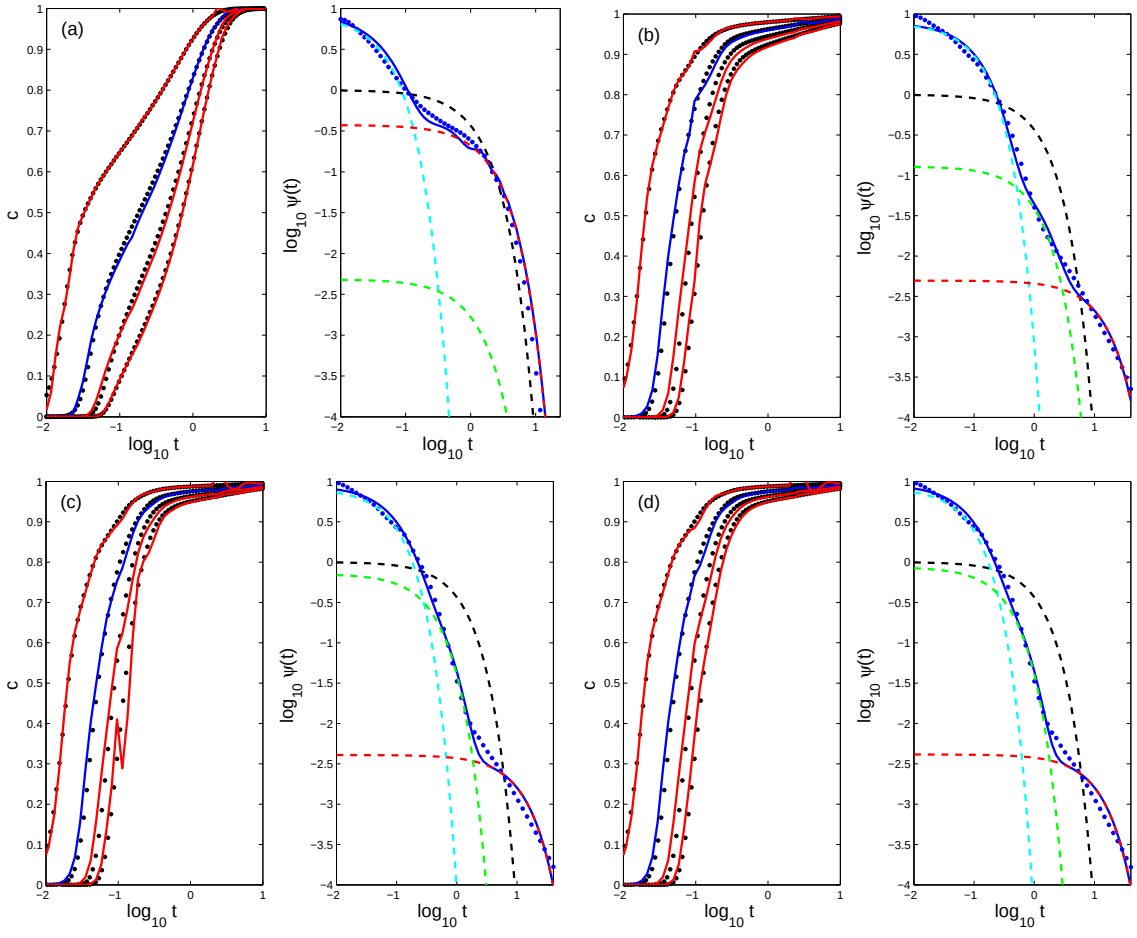

Figure 6. Same as for Figure 5 but for fractures with variable aperture. Opposite to the case of constant aperture, the the non-parametric best-fit $\psi(t)$ (black dots) cannot be represented as the sum of three decaying exponentials. The numerical errors for case (c) at $x = 1$ are due to yet unresolved numerical problem in the inverse Laplace transform algorithm [Cortis and Berkowitz, 2005]. Current work is on the way to improve on the stability of the inversion algorithm.

DISCLAIMER

This document was prepared as an account of work sponsored by the United States Government. While this document is believed to contain correct information, neither the United States Government nor any agency thereof, nor The Regents of the University of California, nor any of their employees, makes any warranty, express or implied, or assumes any legal responsibility for the accuracy, completeness, or usefulness of any information, apparatus, product, or process disclosed, or represents that its use would not infringe privately owned rights. Reference herein to any specific commercial product, process, or service by its trade name, trademark, manufacturer, or otherwise, does not necessarily constitute or imply its endorsement, recommendation, or favoring by the United States Government or any agency thereof, or The Regents of the University of California. The views and opinions of authors expressed herein do not necessarily state or reflect those of the United States Government or any agency thereof or The Regents of the University of California.

Ernest Orlando Lawrence Berkeley National Laboratory is an equal opportunity employer.